physchem

MDPI

Article

Substituent Effects on the Photophysical Properties of a Series of 8(*meso*)-Pyridyl-BODIPYs: A Computational Analysis of the Experimental Data †

Petia Bobadova-Parvanova [1,*], Dylan Goliber [1], Elijuah Hernandez [1], Daniel LaMaster [2] and Maria da Graça H. Vicente [3]

[1] Department of Chemistry and Fermentation Sciences, Appalachian State University, Boone, NC 28608, USA; goliberda@appstate.edu (D.G.); hernandezej@appstate.edu (E.H.)
[2] Department of Chemistry, Talladega College, Talladega, AL 35160, USA; dlamaster@tallageda.edu
[3] Department of Chemistry, Louisiana State University, Baton Rouge, LA 70803, USA; vicente@lsu.edu
* Correspondence: bobadovap@appstate.edu

† Part of the material was presented at the ACS National Meeting, New Orleans, LA, USA, 17–21 March 2024, 22nd MERCURY Conference, Merced, CA, USA, 14–19 July 2024, and 75th SERMACS, Atlanta, GA, USA, 23–26 October 2024.

Abstract: Recently, a series of 8(*meso*)-pyridyl-BODIPYs (2-pyridyl, 3-pyridyl, and 4-pyridyl) and their 2,6-substituted derivatives were synthesized and their structure and photophysical properties were studied both experimentally and computationally. One of the main observed trends was that the 2-pyridyl-BODIPYs were consistently less fluorescent than their 3-pyridyl and 4-pyridyl analogs, regardless of the 2,6-substituents. Herein, we extend our previous computational studies and model not only the ground but also the excited states of the entire series of previously synthesized *meso*-pyridyl-BODIPYs with the aim of explaining the observed differences in the emission quantum yields. To better understand the trends and the effect of 2- and 2,6-substitution on the photophysical and electron-density-related properties, we also model the ground and excited states of BODIPYs that were not synthesized experimentally, however represent a logical part of the series. We calculate a variety of molecular properties and propose that the experimentally observed low quantum yields for all 2-pyridyl-BODIPYs could be due to the very flat potential energy surfaces with respect to the rotation of the 2-pyridyl ring in the excited states, and the stability of a non-planar and significantly less fluorescent *meso*-2-pyridyl-BODIPY structure.

Keywords: BODIPY; pyridyl; fluorescence; rotation; substituent effect

Citation: Bobadova-Parvanova, P.; Goliber, D.; Hernandez, E.; LaMaster, D.; Vicente, M.d.G.H. Substituent Effects on the Photophysical Properties of a Series of 8(*meso*)-Pyridyl-BODIPYs: A Computational Analysis of the Experimental Data. *Physchem* **2024**, *4*, 483–494. https://doi.org/10.3390/physchem4040034

Academic Editor: James A. Platts

Received: 4 October 2024
Revised: 7 November 2024
Accepted: 14 November 2024
Published: 29 November 2024

1. Introduction

Boron dipyrromethene (BODIPY)-based fluorophores have attracted significant research attention in the last several decades [1–6] and have found a wide range of applications, including as medical imaging agents [7–10], biological labels [11,12], photosensitizers in cancer therapy [13–15], fluorescence switches [16,17], and laser dyes [18–20]. They have been shown to exhibit excellent physicochemical properties, among which are sharp absorption and emission bands in the visible region, high-fluorescence quantum yields, and high photo- and chemical stability [1–6]. One of the major advantages of BODIPYs is that they can be functionalized at all the carbon atoms and at the boron center (Figure 1), enabling the fine tuning of their chemical and photophysical properties toward a particular application [4,5,20,21]. This is particularly interesting from a computational chemistry point of view because the design and synthesis of BODIPY fluorophores with pre-determined physicochemical properties could be greatly simplified if it is possible to find a molecular descriptor that is related to the property of interest [22].

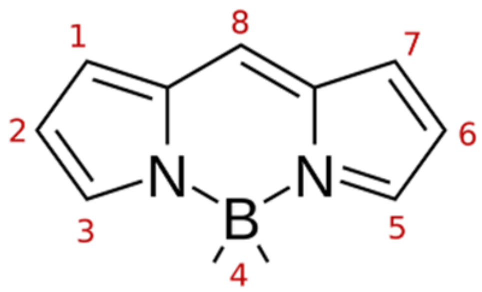

Figure 1. Potential functionalization sites in BODIPYs. In the present study, we focus on 8(*meso*)-pyridyl substitution and 2- and 2,6-substitution with electron-withdrawing groups (Cl, NO_2, CO_2Me, CF_3).

Of the various BODIPY derivatives, 8(*meso*)-pyridyl-substituted BODIPYs have attracted research interest because of the straightforward protonation or alkylation of the pyridyl groups, which allows the synthesis of low-molecular-weight water-soluble fluorescent dyes [23,24]. Recently, a series of *meso*-(2-, 3-, and 4-pyridyl)-BODIPYs (Figure 2) and their 2- and 2,6-substituted analogs was studied both experimentally and computationally [25,26]. The electron-withdrawing chloro-, nitro-, and methoxycarbonyl groups were used and their effect on the photophysical properties of the respective dyes were studied systematically. One of the main observed trends was that the 2-pyridyl-BODIPYs were consistently less fluorescent that their 3- and 4-pyridyl analogs. The reason for this interesting behavior was not found. Furthermore, the change in photophysical properties with the substitution of each electron-withdrawing group varied substantially. The introduction of a chloro substituent increased the fluorescence quantum yield, while the introduction of a nitro substituent quenched the fluorescence.

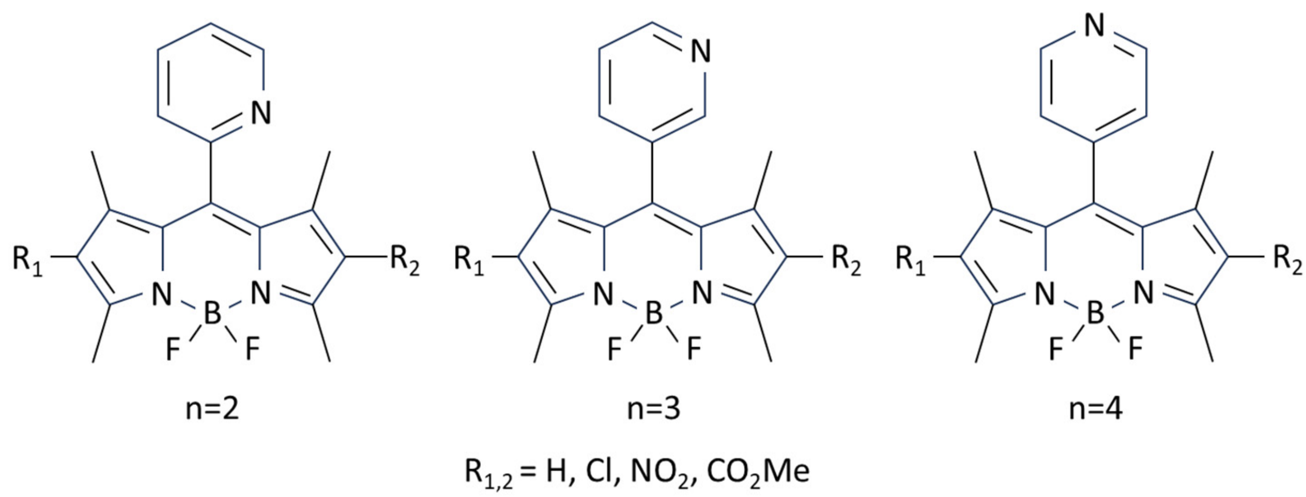

Figure 2. Experimentally synthesized *meso*-(2-, 3-, and 4-pyridyl)-BODIPYs: **nPy**, **nPyCl$_2$**, **nPyNO$_2$**, **nPyNO$_2$Cl**, and **nPy(CO$_2$Me)$_2$**, where n = 2, 3, 4.

Herein, we extend our previous computational studies and model not only the ground but also the excited states of the entire series of previously synthesized *meso*-(2-, 3-, and 4-pyridyl)-BODIPYs with the aim to explain the observed drastic differences in the emission quantum yields of the dyes. To better understand the trends and the effect of 2- and 2,6-substitution on their photophysical and electron-density related properties, we also model the ground and excited states of compounds not yet synthesized experimentally, however represents a logical part of the series. These are the mono- or di-substituted analogs of the experimentally synthesized compounds, and BODIPYs with $R_{1,2}$ = CF_3, as a strongly σ-bond electron-withdrawing group. Thus, the entire series studied includes **nPy**, **nPyCl**, **nPyCl$_2$**, **nPyNO$_2$**, **nPy(NO$_2$)$_2$**, **nPyCO$_2$Me**, **nPy(CO$_2$Me)$_2$**, **nPyCF$_3$**, and **nPy(CF$_3$)$_2$**, where n = 2, 3, 4. Among these, the **nPy**, the mono-substituted **nPyNO$_2$**, and the di-substituted **nPyCl$_2$** and **nPy(CO$_2$Me)$_2$** have been previously synthesized experimentally and reported in Refs. [25,26]. To analyze the effect of *meso*-pyridyl substitution, we also included the *meso*-phenyl analogs **Phe**, **PheCl**, **PheCl$_2$**, **PheNO$_2$**, **Phe(NO$_2$)$_2$**, **PheCO$_2$Me**, **Phe(CO$_2$Me)$_2$**, **PheCF$_3$**, and **Phe(CF$_3$)$_2$**.

2. Computational Methods

The geometries of the ground and excited states of all compounds studied were optimized without symmetry constraints at the cam-b3lyp [27] /6-31+G(d,p) level in vacuum. Not including the solvent effects in the calculations could be considered a limitation. However, a previous detailed study has shown that using the cam-b3lyp [27] /6-31+G(d,p) level in vacuum correctly reproduced the experimental trends and the ordering of the molecular orbitals in *meso*-(4-pyridyl)-BODIPYs [23].

The UV-vis absorption and emission data were calculated using the TD-DFT [28] /cam-b3lyp/6-31+G(d,p) method in vacuum. The range-separated cam-b3lyp functional was used to capture the long-range interactions in the transitions between the BODIPY core and the pyridyl ring. The first three singlet excitations were considered, and the lowest-energy excited singlet state was optimized to calculate the energies, atomic charges, dipole moments, maximum emission wavelengths, and the other properties reported in this manuscript. The potential energy minima of the ground and excited states were confirmed with frequency calculations.

All calculations were performed using the Gaussian 09 program package [29].

3. Results and Discussion

3.1. Photophysical Properties

The calculated photophysical properties of the entire series of *meso*-(2-, 3-, and 4-pyridyl)-BODIPYs are presented in Table 1. The experimentally measured data are given when available. The dominant transition for all studied BODIPYs is $\mathbf{S_0{\rightarrow}S_1}$. The next singlet excited state is more than 0.9 eV higher in energy and, therefore, has minimal contribution. A previously study from our laboratory [25,26] reported that the experimentally measured maximum absorption (λ_{abs}) and emission (λ_{em}) wavelengths for **nPy**, **nPyNO$_2$**, **nPyCl$_2$**, and **nPy(CO$_2$Me)$_2$** are almost identical within a given n = 2, 3, 4 series bearing the same 2,6-substituents. It was determined that this was related to the almost identical HOMO-LUMO gaps of the ground states for a given series. As seen in Table 1, the newly calculated hypothetical compounds **nPyCl**, **nPy(NO$_2$)$_2$**, **nPyCO$_2$Me**, **nPyCF$_3$**, and **nPy(CF$_3$)$_2$**, where n = 2, 3, 4, show similar trends—λ_{abs} and λ_{em} are almost identical within a given n = 2, 3, 4 series. It is hypothesized that such trends will be observed regardless of the 2,6-substituents on the *meso*-(2-, 3-, and 4-pyridyl)-BODIPYs.

As could be expected, the computationally determined λ_{abs} and λ_{em} are significantly blue-shifted, as a known tendency of TD-DFT methods to overestimate singlet-singlet excitation energies [30,31]. However, the similarities in the experimentally observed λ_{abs} and λ_{em} within a series correlate very well with the similarities in the TD-DFT computational values. In addition, the experimentally observed red-shifts upon chlorination and blue-shifts upon nitration are in agreement with the calculated λ_{abs} and λ_{em} values. All these suggest that the computed λ_{abs} and λ_{em} can be used to determine the observed trends in the experimental data.

As previously observed [25,26], the experimental fluorescence properties of *meso*-(2-, 3-, and 4-pyridyl)-BODIPYs largely depend on the relative position of the nitrogen atom on the pyridine ring. The *meso*-(2-pyridyl)-BODIPY derivatives consistently show the lowest fluorescence quantum yields within an n = 1, 2, 3 series. This trend is valid in all experimentally observed values and is regardless of the substituents at the 2,6-positions. We will attempt to explain this phenomenon in the next sections.

Table 1. Experimental and calculated photophysical properties of *meso*-(2-, 3-, and 4-pyridyl)-BODIPYs: maximum absorption wavelength (λ_{abs}), oscillator strength (f), maximum emission wavelength (λ_{em}), and quantum yield (Φ).

***meso*-BODIPY**	**λ_{abs} (nm)**		**f**	**λ_{em} (nm)**		**Φ**
	exp	**calc**		**exp**	**calc**	
Phe	501 (498) [a]	414	0.539	505 (508) [a]	426	0.56 (0.65) [a]
2Py	502 [b]	416	0.542	514 [b]	441	0.04 [b]
3Py	502 [b]	416	0.542	514 [b]	429	0.43 [b]
4Py	501 [b]	415	0.543	515 [b]	428	0.31 [b]
PheCl		434	0.508		437	
2PyCl		424	0.552		446	
3PyCl		424	0.551		441	
4PyCl		423	0.551		443	
$PheCl_2$		430	0.561		447	
$2PyCl_2$	530 [b]	432	0.565	545 [b]	455	0.17 [b]
$3PyCl_2$	527 [b]	432	0.565	542 [b]	452	0.58 [b]
$4PyCl_2$	528 [b]	432	0.566	546 [b]	454	0.58 [b]
$PheNO_2$		405	0.659		425	
$2PyNO_2$	491 [c]	408	0.655	509 [c]	436	0.05 [c]
$3PyNO_2$	491 [c]	407	0.656	507 [c]	429	0.25 [c]
$4PyNO_2$	490 [c]	406	0.660	508 [c]	431	0.26 [c]
$Phe(NO_2)_2$		409	0.677		434	
$2Py(NO_2)_2$		413	0.673		443	0.13
$3Py(NO_2)_2$		412	0.675		438	0.28
$4Py(NO_2)_2$		412	0.676		440	0.36
$PheCO_2Me$		410	0.658		427	
$2PyCO_2Me$		413	0.658		441	0.21
$3PyCO_2Me$		413	0.659		431	0.61
$4PyCO_2Me$		412	0.661		435	0.39
$Phe(CO_2Me)_2$		410	0.791		426	
$2Py(CO_2Me)_2$	501 [c]	413	0.797	515 [c]	436	0.09
$3Py(CO_2Me)_2$	501 [b]	413	0.793	512 [c]	430	0.61
$4Py(CO_2Me)_2$	500 [b]	412	0.794	510 [c]	434	0.43
$PheCF_3$		407	0.594		425	
$2PyCF_3$		409	0.596		437	
$3PyCF_3$		409	0.597		429	
$4PyCF_3$		408	0.599		432	
$Phe(CF_3)_2$		404	0.6605		424	
$2Py(CF_3)_2$		406	0.6639		434	
$3Py(CF_3)_2$		406	0.6645		428	
$4Py(CF_3)_2$		406	0.667		418	

[a] From Ref. [32] in THF and Ref. [1] in methanol. [b] From Ref. [25] in acetonitrile. [c] From Ref. [26] in acetonitrile.

3.2. Electron-Density-Related Properties of the Ground and Excited States

The apparent difference between *meso*-(2-pyridyl)- and *meso*-(3-, and 4-pyridyl)-BODIPYs is the closer proximity of the nitrogen atom to the BODIPY core in the former compounds. The different positions of the nitrogen atom in the pyridyl group result in different strengths of the electron-withdrawing effect of the pyridyl nitrogen and different electron densities in these compounds. To evaluate these differences, we analyzed the shapes and the energies of the frontier molecular orbitals. We also analyzed the dipole moments and their changes upon excitation.

The shapes of the frontier molecular orbitals (Figure 3, Figure S1, Supplementary Materials) clearly demonstrate that the electron-withdrawing effect of the substituent featuring electron density spread to Cl, NO_2, CO_2Me, and CF_3 moieties, respectively. This is observed in both S_0 and S_1 states. However, regardless of the substituent, both HOMO and LUMO are almost entirely localized on the BODIPY core, indicating no significant charge-transfer effect and no drastic difference between *meso*-(2-pyridyl)-BODIPYs and *meso*-(3-, and 4-pyridyl)-BODIPYs. Thus, while the frontier molecular orbitals clearly indicate the effect of different electron-withdrawing substituents at the 2,6 positions, they cannot explain the drastic difference in the experimentally observed fluorescence quantum yield between *meso*-(2-pyridyl)-BODIPYs and their *meso*-(3-, and 4-pyridyl)-analogs.

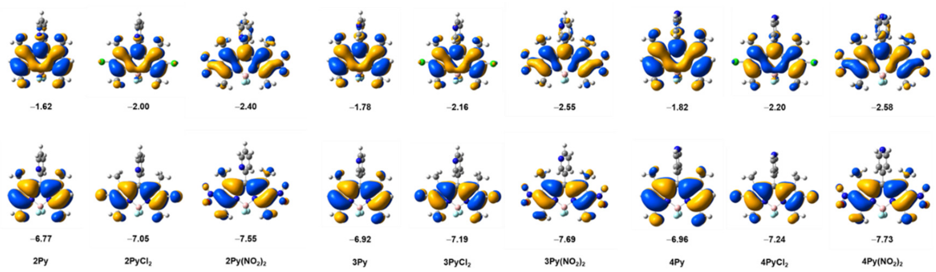

Figure 3. Frontier molecular orbitals of 2,6-unsubstituted, di-chlorinated and di-nitrated *meso*-(2-, 3-and 4-pyridyl)-BODIPYs. The frontier orbitals of the complete 2,6-di-substituted series are given in Figure S1, Supplementary Materials. Orbital energies in eV.

The energies of the HOMO and LUMO for the ground states of all studied compounds are given in Table 2. As expected, both HOMO and LUMO are stabilized upon 2- and 2,6-substituion with electron-withdrawing groups, with the di-substituted compounds showing a greater effect. The stabilization is most pronounced in the case of nitration and least pronounced in the case of chlorination. All n = 2, 3, 4 series follow the same trends when compared to the *meso*-phenyl analogs. *Meso*-2-pyridyl substitution has a slight effect on HOMO (a destabilization by only 0.02–0.03 eV), while *meso*-(3- and 4-pyridyl)-substitutions stabilize HOMO by 0.1–0.2 eV. The effect of *meso*-(3- and 4-pyridyl)-substitution is almost identical but consistently features 0.04 eV lower HOMO energies in the case of *meso*-4-pyridyl-BODIPYs. The effect on LUMO is consistent stabilization, which is almost negligible in the case of *meso*-2-pyridyl substitution (0–0.1 eV) and significantly more pronounced in the case of *meso*-(3-, and 4-pyridyl)-substitution (0.14–0.16 eV). Again, the effect is slightly greater for *meso*-4-pyridyl than for *meso*-3-pyridyl. The analysis of the HOMO and LUMO energies demonstrates that the effect of *meso*-n-pyridyl substitution is similar for n = 3,4 but different in the case of n = 2. This might be related to the observed quantum yield differences.

Table 2 also lists the calculated dipole moments for the ground states and the scalar ($\Delta\mu = \mu_1 - \mu_0$) and vector ($\overrightarrow{\Delta\mu} = \left|\overrightarrow{\mu_1} - \overrightarrow{\mu_0}\right|$) changes in the dipole moment upon excitation, where the subscript 0 refers to the ground state and subscript 1 refers to the first singlet excited state of the respective compound. Analysis of the magnitude of the dipole moment (μ_0) indicates that the *meso*-2-pyridyl-BODIPYs are consistently the most polar and the *meso*-4-pyridyl-BODIPYs are consistently the least polar BODIPYs within a given n = 2, 3, 4 series. The *meso*-2-pyridyl-BODIPYs are also consistently more polar than their *meso*-phenyl analogs. These two trends exist in both the S_0 and S_1 states, regardless of the 2,6-substituent. Interestingly, upon excitation, the dipole moment decreases in the mono-2-substituted BODIPYs but increases in the 2,6-di-substituted BODIPYs. The change in polarity upon excitation depends on the 2,6-substituent—it is most pronounced for nitration and least pronounced for chlorination. Whether this is related to the fact that chlorination increases the experimental quantum yield, while nitration decreases it, is currently under study in our laboratory.

Table 2. Calculated ground-state HOMO and LUMO energies, band gap ($E_{g,0}$), dipole moment (μ_0), and the scalar ($\Delta\mu = \mu_1 - \mu_0$) and absolute value of the vector change ($\Delta\vec{\mu} = \left|\vec{\mu_1} - \vec{\mu_0}\right|$) of the dipole moment upon excitation for the series of *meso*-pyridyl-BODIPYs studied. The subscript 0 refers to the ground state and the subscript 1 refers to the first singlet excited state.

BODIPY	$HOMO_0$ (eV)	$LUMO_0$ (eV)	$E_{g,0}$ (eV)	μ_0 (D)	$\Delta\mu$ (D)	$\Delta\vec{\mu}$ (D)
Phe	−6.79	−1.62	5.17	5.03	0.07	0.07
2Py	−6.77	−1.62	5.14	6.05	0.03	0.05
3Py	−6.92	−1.78	5.14	3.94	0.02	0.08
4Py	−6.96	−1.82	5.15	2.13	0.02	0.07
PheCl	−6.94	−1.82	5.12	5.61	0.13	0.29
2PyCl	−6.91	−1.82	5.10	6.53	−0.08	0.10
3PyCl	−7.06	−1.97	5.09	4.53	−0.04	0.22
4PyCl	−7.10	−2.01	5.10	3.14	0.08	0.16
PheCl$_2$	−7.07	−2.01	5.07	5.23	0.20	0.27
2PyCl$_2$	−7.05	−2.00	5.05	6.22	0.16	0.58
3PyCl$_2$	−7.19	−2.15	5.04	4.02	0.28	0.53
4PyCl$_2$	−7.23	−2.19	5.04	2.30	0.14	0.14
PheNO$_2$	−7.46	−2.21	5.25	9.04	−0.33	0.45
2PyNO$_2$	−7.44	−2.22	5.21	9.51	−0.58	0.87
3PyNO$_2$	−7.58	−2.37	5.21	8.02	−0.60	0.71
4PyNO$_2$	−7.62	−2.40	5.22	7.54	−0.41	0.46
Phe(NO$_2$)$_2$	−8.01	−2.80	5.21	6.09	0.17	0.17
2Py(NO$_2$)$_2$	−7.98	−2.81	5.17	7.08	0.14	0.41
3Py(NO$_2$)$_2$	−8.13	−2.96	5.17	4.91	0.15	0.28
4Py(NO$_2$)$_2$	−8.17	−3.00	5.18	3.11	0.11	0.11
PheCO$_2$Me	−7.03	−1.83	5.21	3.98	0.02	0.39
2PyCO$_2$Me	−7.01	−1.83	5.18	4.86	−0.30	0.71
3PyCO$_2$Me	−7.16	−1.99	5.17	3.02	−0.38	0.61
4PyCO$_2$Me	−7.20	−2.02	5.18	1.92	−0.07	0.35
Phe(CO$_2$Me)$_2$	−7.24	−2.02	5.22	1.92	0.11	0.11
2Py(CO$_2$Me)$_2$	−7.21	−2.02	5.19	3.00	0.16	0.42
3Py(CO$_2$Me)$_2$	−7.36	−2.18	5.18	1.89	0.04	0.31
4Py(CO$_2$Me)$_2$	−7.40	−2.21	5.19	1.05	−0.03	0.03
PheCF$_3$	−7.20	−1.97	5.24	6.78	−0.04	0.18
2PyCF$_3$	−7.18	−1.97	5.21	7.56	−0.36	0.71
2PyCF$_3$	−7.33	−2.13	5.21	5.85	−0.32	0.53
2PyCF$_3$	−7.37	−2.16	5.21	4.87	−0.11	0.18
Phe(CF$_3$)$_2$	−7.57	−2.31	5.26	5.43	0.14	0.14
2Py(CF$_3$)$_2$	−7.54	−2.31	5.24	6.46	0.03	0.61
3Py(CF$_3$)$_2$	−7.69	−2.46	5.23	4.30	0.13	0.47
4Py(CF$_3$)$_2$	−7.73	−2.49	5.24	2.50	0.11	0.11

Next, we look at the orientation of the dipole moment. Since nitrogen is more electronegative than carbon, the different position of the pyridyl nitrogen will create a different orientation of the dipole moment vector. Figure 4 shows a side view of the dipole moment vectors for the 2,6-dichlorinated and 2,6-dinitrated *meso*-(2-, 3-, and 4-pyridyl)-BODIPYs, as two examples of the effect. The *meso*-phenyl-BODIPY analogs and the unsubstituted BODIPYs are included for comparison. All compounds were optimized without symmetry constrains; however, for simplicity, we will refer to pseudo symmetry elements to explain the vector orientations. As with all di-substituted BODIPYs, the dipole moments lie in the pseudo mirror plane of symmetry (if the molecule was symmetric), i.e., the plane of the 2D representation in Figure 4. The *meso*-(4-pyridyl)-BODIPYs have their dipole moments oriented along a pseudo C_2 axis (if the molecule was symmetric). The *meso*-(2-, and

3-pyridyl)-BODIPYs have their dipole moments oriented at an angle of roughly 30° for *meso*-(2-pyridyl)-BODIPYs and roughly 60° for *meso*-(3-pyridyl)-BODIPYs with respect to the pseudo C_2 axis.

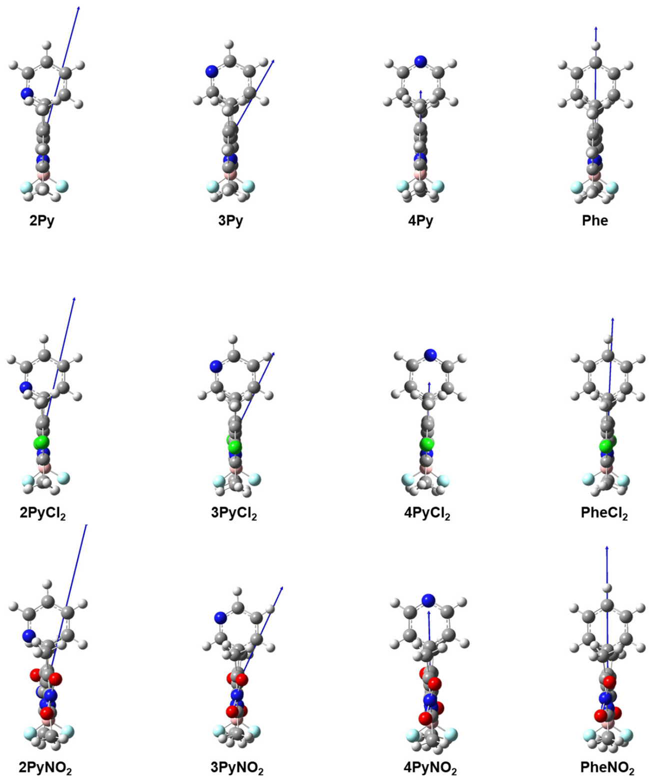

Figure 4. Side view of the dipole moments of 2,6-unsubstituted, 2,6-dichlorinated, and 2,6-dinitrated *meso*-(2-, 3-, and 4-pyridyl)-BODIPYs compared with the *meso*-phenyl-BODIPY analog. All dipole moments lie in the pseudo mirror plane of symmetry (the plane of the 2D representation in this figure). The *meso*-2-pyridyl-BODIPYs are consistently most polar regardless of the 2,6-substituent.

According to a recent study of a series of conjugated terpyridine derivatives [22], the fluorescence quantum yield could be quantified by the change in dipole moment between the ground and excited states. To check the applicability of this approach for our series, we calculated the absolute value of the vector change in the dipole moment ($\overrightarrow{\Delta\mu} = \left|\overrightarrow{\mu_1} - \overrightarrow{\mu_0}\right|$) upon excitation. These data are presented in the last column of Table 2. For almost all 2,6-substituents, the $\overrightarrow{\Delta\mu}$ value suggests the greatest quantum yield for *meso*-(2-pyridyl)-BODIPYs, which contradicts the experimental findings. The observed significant decrease in the fluorescence of *meso*-(2-pyridyl)-BODIPYs must be due to a different reason.

3.3. Rotational Barrier in the Excited States

As mentioned above, the major difference between the *meso*-(2-pyridyl) and *meso*-(3- and 4-pyridyl)-BODIPYs is the closer proximity of the nitrogen atom of the pyridine group to the BODIPY core in the former compounds. In addition to the different strengths of the electron-withdrawing effect of the pyridyl nitrogen and the different electron densities, the different positions of the nitrogen atom result in different steric effects. In *meso*-(2-pyridyl) compounds, position 2 is occupied by a nitrogen atom but in *meso*-(3- and 4-pyridyl)-BODIPYs it is occupied by a carbon atom bonded to a hydrogen atom. Because of the methyl groups in the 1,7-positions for the entire series studied, this could affect the rotation of the pyridyl ring. We hypothesized that the 2-pyridyl ring might be easier to rotate than the 3- and 4-pyridyl rings.

Analysis of the geometries of the ground states shows that the *meso*-pyridyl ring is oriented approximately perpendicular with respect to the BODIPY core (≈ 90°) for all but the mono- and di-nitro compounds (Table S1, Supplementary Materials). This orientation is consistent with the experimental findings for the crystal structure of the previously synthesized BODIPYs from the series [26]. The slight difference in the case of **2PyNO$_2$**, **3PyNO$_2$**, and **4PyNO$_2$** is also consistent with the experiment and could be related to the lower fluorescence quantum yields observed in the case of these compounds compared to the other BODIPYs from the series, which is likely due to partial delocalization of LUMO to the pyridyl ring (Figure 3).

Similar analysis in the case of the excited states demonstrates that the *meso*-pyridyl ring forms different dihedral angles with the BODIPY core that do not necessarily follow a trend (Table S1, Supplementary Materials). For this reason, we decided to concentrate on the analysis of the excited states and the differences in the rotation of the 2-, 3-, and 4-pyridyl rings upon excitation.

We modeled the rotation of the *meso*-pyridyl group and estimated the rotational barrier in the excited states in the cases of the 2,6-unsubstituted *meso*-(2-, 3-, and 4-pyridyl)-BODIPYs. The results of the scan are shown in Figure 5. In the case of *meso*-(3-pyridyl and 4-pyridyl)-BODIPYs, the potential energy surfaces of the *meso*-rotation in the excited states are very flat. All energies required for the rotation up to 40° are lower compared to the roughly 20 kcal/mol barrier that could be overcome at room temperature. Therefore, we believe that, at room temperature, the *meso*-pyridyl ring rotates freely (Figure 5a). In the case of **3Py** and **4Py**, this rotation causes gradual structural changes. The BODIPY core becomes slightly distorted with the gradually increasing contribution of the pyridyl ring to LUMO, as the *meso*-dihedral angle, θ, decreases. This is reflected in a gradual red-shift in the maximum emission wavelength, λ_{em}, and a slight decrease in the oscillator strength (Figure 5b,c). In the case of **2Py**, however, when θ approaches 40°, the structure of the molecule becomes significantly distorted (Figure 6). The BODIPY core is no longer planar and the **2Py** ring becomes tilted. The LUMO drops by 0.7 eV, λ_{em} shifts by almost 80 nm, and the oscillator strength drops significantly (Figure 5b,c).

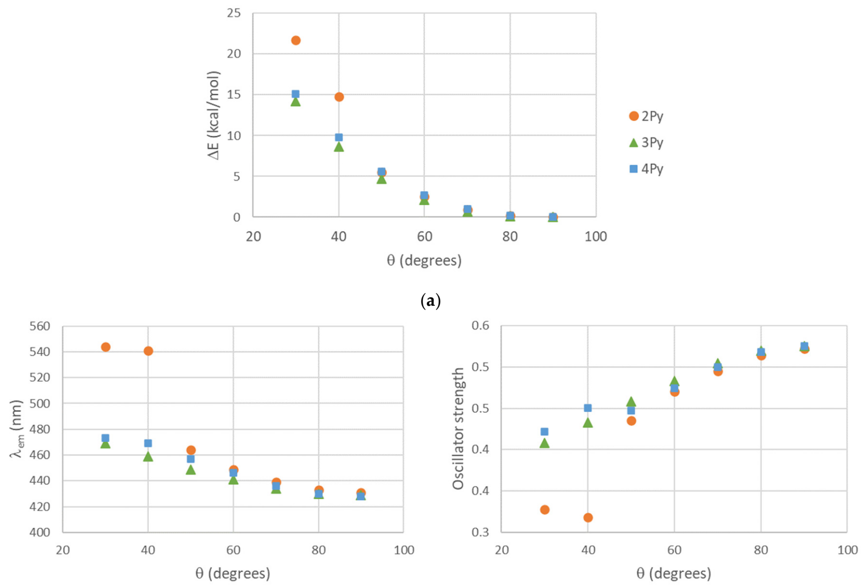

(**a**) (**b**) (**c**)

Figure 5. Energies required for rotation (**a**), maximum emission wavelengths, λ_{em} (**b**), and oscillator strengths (**c**) for the S_1 excited states of **2Py, 3Py**, and **4Py** as a function of the angle of *meso*-pyridyl rotation. Parts of this figure were presented at the ACS National Meeting, New Orleans, LA, USA, 17–21 March 2024 [33], 22nd MERCURY Conference, Merced, CA, USA, 14–19 July 2024 [34], and 75th SERMACS, Atlanta, GA, USA, 23–26 October 2024.

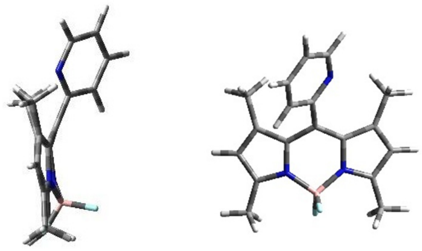

(**a**) (**b**)

Figure 6. Side view (**a**) and front view (**b**) of the lowest-energy structure for the S_1 excited state of **2Py** when the *meso*-dihedral angle, θ, is kept fixed at 40°.

An explanation for the significant drop in the oscillator strength can be seen in Figure 7. When $\theta = 90°$, almost the entire electron density is localized on the BODIPY core and the molecule will fluoresce. However, as the *meso*-dihedral angle, θ, decreases, the electron density becomes delocalized onto the pyridyl ring, indicating a gradual increase in the charge transfer effect that lowers the fluorescence. This is observed until θ reaches 40°, when the distorted structure bearing a non-planar, non-fluorescent BODIPY core and tilted pyridyl ring becomes the lowest-energy conformation. We propose that this effect is the reason for the experimentally observed drastic decrease in the fluorescence of **2Py**. Indeed, similar distorted structures exist in the case of **3Py** and **4Py**; however, they are very high in energy, 31 kcal/mol and 61 kcal/mol, respectively, compared to the roughly 20 kcal/mol barrier that could be overcome at room temperature. Therefore, these structures do not significantly affect the fluorescence of **3Py** and **4Py** to the same extent as for **2Py**, where the distorted structure is located only 15 kcal/mol above the $\theta = 90°$ minimum.

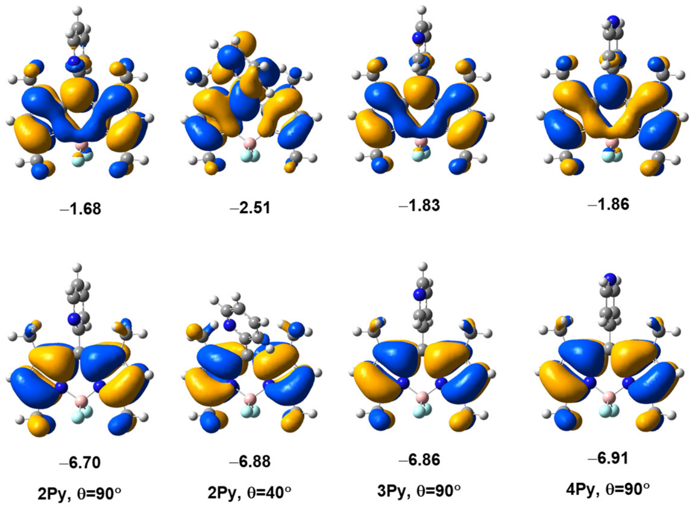

Figure 7. Frontier orbitals of the S_1 excited states of unsubstituted *meso*-(2-, 3- and 4-pyridyl)-BODIPYs at different *meso*-dihedral angles of the pyridyl ring with respect to the BODIPY core, θ. Orbital energies in eV. Parts of this figure were presented at the ACS National Meeting, New Orleans, LA, USA, 17–21 March 2024 [33], 22nd MERCURY Conference, Merced, CA, USA, 14–19 July 2024 [34], and 75th SERMACS, Atlanta, GA, USA, 23–26 October 2024.

4. Conclusions

The performed computational modeling of a series of *meso*-(2-, 3-, and 4-pyridyl)-BODIPYs and their *meso*-phenyl analogs allows for several conclusions to be drawn.

Electron-withdrawing substituents at the 2,6-positions lower both HOMO and LUMO and affect both the energies and the shapes of the molecular orbitals. The calculated HOMO-LUMO gaps correlate with the experimentally observed red- or blue-shifts in the maximum absorption and emission wavelengths.

The analysis of the HOMO and LUMO energies demonstrates that the effect of *meso*-pyridyl substitution is significantly more pronounced for the 3- and 4-pyridyl-BODIPYs compared to their 2-pyridyl analogs.

The excited states are consistently less polar than the ground states in all 2-mono-substituted BODIPYs. The change in polarity upon excitation depends on the 2,6-substituent(s)—it is most pronounced for nitration and least pronounced for chlorination.

The experimentally observed consistent low quantum yields for the *meso*-(2-pyridyl) BODIPYs could be due to the very flat potential energy surfaces with respect to rotation of the 2-pyridyl ring in the excited states, and the stability of a crooked, non-planar, and significantly less fluorescent *meso*-(2-pyridyl) excited state structure.

The results from this study might be used to investigate other fluorescence quenching effects in fluorophores that might be due to structural changes in the excited states. Scanning the PES of the excited states of other BODIPYs might provide more insight into the mechanism of fluorescence quenching when no charge-transfer quenching occurs. It would also be interesting to account for the low-energy vibrational soft modes and examine their effects on the absorption and emission spectra of the compounds.

Supplementary Materials: The following supporting information can be downloaded at https://www.mdpi.com/article/10.3390/physchem4040034/s1: Figure S1: Frontier molecular orbitals of the series of disubstituted *meso*-(2-, 3-, and 4-pyridyl)-BODIPYs. Table S1: CAM-B3LYP/6-31+G(d,p) calculated Natural Population Analysis (NPA) atomic charge of the *meso*-carbon, Molecular Electrostatic Potentials (MESPs) of the *meso*-carbon, and pyridyl dihedral angle with respect to the BODIPY core for the ground (S_0) and first singlet excited state (S_1) of the series of BODIPYs studied.

Author Contributions: Conceptualization, P.B.-P., D.L. and M.d.G.H.V.; methodology, P.B.-P. and D.L.; software, P.B.-P., D.G. and E.H.; validation, P.B.-P., D.G. and E.H.; formal analysis, P.B.-P. and M.d.G.H.V.; investigation, P.B.-P., D.L. and M.d.G.H.V.; resources, P.B.-P. and M.d.G.H.V.; data curation, P.B.-P., D.G. and E.H.; writing—original draft preparation, P.B.-P. and D.G.; writing—review and editing, P.B.-P., D.L., D.G. and M.d.G.H.V.; visualization, P.B.-P.; supervision, P.B.-P. and M.d.G.H.V.; project administration, P.B.-P. and M.d.G.H.V.; funding acquisition, P.B.-P. and M.d.G.H.V. All authors have read and agreed to the published version of the manuscript.

Funding: This research was funded by the National Science Foundation, grant number CHE-2055190.

Data Availability Statement: Data are contained within the article and Supplementary Materials.

Acknowledgments: The authors are thankful to the Louisiana State University High Performance Computing Center (http://www.hpc.lsu.edu) for use of its computational resources in conducting this research. P.B.P. is grateful for the membership in the MERCURY consortium, which receives support through the National Science Foundation, grant number CHE 2320718.

Conflicts of Interest: The authors declare no conflicts of interest. The funders had no role in the design of the study; in the collection, analyses, or interpretation of data; in the writing of the manuscript, or in the decision to publish the results.

References

1. Loudet, A.; Burgess, K. BODIPY Dyes and Their Derivatives: Syntheses and Spectroscopic Properties. *Chem. Rev.* **2007**, *107*, 4891–4932. [CrossRef] [PubMed]
2. Krumova, K.; Cosa, G. Bodipy Dyes with Tunable Redox Potentials and Functional Groups for Further Tethering: Preparation, Electrochemical, and Spectroscopic Characterization. *J. Am. Chem. Soc.* **2010**, *132*, 17560–17569. [CrossRef] [PubMed]
3. Mula, S.; Ray, A.K.; Banerjee, M.; Chaudhuri, T.; Dasgupta, K.; Chattopadhyay, S. Design and Development of a New Pyrromethene Dye with Improved Photostability and Lasing Efficiency: Theoretical Rationalization of Photophysical and Photochemical Properties. *J. Org. Chem.* **2008**, *73*, 2146–2154. [CrossRef] [PubMed]
4. Ulrich, G.; Ziessel, R.; Harriman, A. The Chemistry of Fluorescent Bodipy Dyes: Versatility Unsurpassed. *Angew. Chem. Int. Ed.* **2008**, *47*, 1184–1201. [CrossRef]
5. Bañuelos, J. BODIPY Dye, the Most Versatile Fluorophore Ever? *Chem. Rec.* **2016**, *16*, 335–348. [CrossRef]
6. Poddar, M.; Misra, R. Recent Advances of BODIPY Based Derivatives for Optoelectronic Applications. *Coord. Chem. Rev.* **2020**, *421*, 213462. [CrossRef]

7. Hendricks, J.A.; Keliher, E.J.; Wan, D.; Hilderbrand, S.A.; Weissleder, R.; Mazitschek, R. Synthesis of [^{18}F]BODIPY: Bifunctional Reporter for Hybrid Optical/Positron Emission Tomography Imaging. *Angew. Chem. Int. Ed.* **2012**, *51*, 4603–4606. [CrossRef]
8. Yu, C.; Wu, Q.; Wang, J.; Wei, Y.; Hao, E.; Jiao, L. Red to Near-Infrared Isoindole BODIPY Fluorophores: Synthesis, Crystal Structures, and Spectroscopic and Electrochemical Properties. *J. Org. Chem.* **2016**, *81*, 3761–3770. [CrossRef]
9. Zhao, N.; Williams, T.M.; Zhou, Z.; Fronczek, F.R.; Sibrian-Vazquez, M.; Jois, S.D.; Vicente, M.G.H. Synthesis of BODIPY-Peptide Conjugates for Fluorescence Labeling of EGFR Overexpressing Cells. *Bioconjug. Chem.* **2017**, *28*, 1566–1579. [CrossRef]
10. Zhao, N.; Xuan, S.; Zhou, Z.; Fronczek, F.R.; Smith, K.M.; Vicente, M.G.H. Synthesis and Spectroscopic and Cellular Properties of Near-IR [*a*]Phenanthrene-Fused 4,4-Difluoro-4-Bora-3a,4a-Diaza-*s*-Indacenes. *J. Org. Chem.* **2017**, *82*, 9744–9750. [CrossRef]
11. Erbas-Cakmak, S.; Akkaya, E.U. Toward Singlet Oxygen Delivery at a Measured Rate: A Self-Reporting Photosensitizer. *Org. Lett.* **2014**, *16*, 2946–2949. [CrossRef] [PubMed]
12. Gibbs, J.H.; Zhou, Z.; Kessel, D.; Fronczek, F.R.; Pakhomova, S.; Vicente, M.G.H. Synthesis, Spectroscopic, and in Vitro Investigations of 2,6-Diiodo-BODIPYs with PDT and Bioimaging Applications. *J. Photochem. Photobiol. B* **2015**, *145*, 35–47. [CrossRef] [PubMed]
13. Mao, Z.; Kim, J.H.; Lee, J.; Xiong, H.; Zhang, F.; Kim, J.S. Engineering of BODIPY-Based Theranostics for Cancer Therapy. *Coord. Chem. Rev.* **2023**, *476*, 214908. [CrossRef]
14. Amendoeira, A.F.; Luz, A.; Valente, R.; Roma-Rodrigues, C.; Ali, H.; Van Lier, J.E.; Marques, F.; Baptista, P.V.; Fernandes, A.R. Cell Uptake of Steroid-BODIPY Conjugates and Their Internalization Mechanisms: Cancer Theranostic Dyes. *Int. J. Mol. Sci.* **2023**, *24*, 3600. [CrossRef]
15. Kaufman, N.E.M.; Meng, Q.; Griffin, K.E.; Singh, S.S.; Dahal, A.; Zhou, Z.; Fronczek, F.R.; Mathis, J.M.; Jois, S.D.; Vicente, M.G.H. Synthesis, Characterization, and Evaluation of Near-IR Boron Dipyrromethene Bioconjugates for Labeling of Adenocarcinomas by Selectively Targeting the Epidermal Growth Factor Receptor. *J. Med. Chem.* **2019**, *62*, 3323–3335. [CrossRef]
16. Xu, K.; Zhao, J.; Cui, X.; Ma, J. Photoswitching of Triplet–Triplet Annihilation Upconversion Showing Large Emission Shifts Using a Photochromic Fluorescent Dithienylethene-Bodipy Triad as a Triplet Acceptor/Emitter. *Chem. Commun.* **2015**, *51*, 1803–1806. [CrossRef]
17. Ma, J.; Cui, X.; Wang, F.; Wu, X.; Zhao, J.; Li, X. Photoswitching of the Triplet Excited State of DiiodoBodipy-Dithienylethene Triads and Application in Photo-Controllable Triplet–Triplet Annihilation Upconversion. *J. Org. Chem.* **2014**, *79*, 10855–10866. [CrossRef]
18. Ray, C.; Schad, C.; Moreno, F.; Maroto, B.L.; Bañuelos, J.; Arbeloa, T.; García-Moreno, I.; Villafuerte, C.; Muller, G.; De La Moya, S. BCl_3-Activated Synthesis of COO-BODIPY Laser Dyes: General Scope and High Yields under Mild Conditions. *J. Org. Chem.* **2020**, *85*, 4594–4601. [CrossRef]
19. Waddell, P.G.; Liu, X.; Zhao, T.; Cole, J.M. Rationalizing the Photophysical Properties of BODIPY Laser Dyes via Aromaticity and Electron-Donor-Based Structural Perturbations. *Dyes Pigments* **2015**, *116*, 74–81. [CrossRef]
20. Ortiz, M.J.; Garcia-Moreno, I.; Agarrabeitia, A.R.; Duran-Sampedro, G.; Costela, A.; Sastre, R.; Arbeloa, F.L.; Prieto, J.B.; Arbeloa, I.L. Red-Edge-Wavelength Finely-Tunable Laser Action from New BODIPY Dyes. *Phys. Chem. Chem. Phys.* **2010**, *12*, 7804–7811. [CrossRef]
21. Gómez-Durán, C.F.A.; Esnal, I.; Valois-Escamilla, I.; Urías-Benavides, A.; Bañuelos, J.; López Arbeloa, I.; García-Moreno, I.; Peña-Cabrera, E. Near-IR BODIPY Dyes à La Carte—Programmed Orthogonal Functionalization of Rationally Designed Building Blocks. *Chem.–Eur. J.* **2016**, *22*, 1048–1061. [CrossRef] [PubMed]
22. Humbert-Droz, M.; Piguet, C.; Wesolowski, T.A. Fluorescence Quantum Yield Rationalized by the Magnitude of the Charge Transfer in π-Conjugated Terpyridine Derivatives. *Phys. Chem. Chem. Phys.* **2016**, *18*, 29387–29394. [CrossRef] [PubMed]
23. LaMaster, D.J.; Kaufman, N.E.M.; Bruner, A.S.; Vicente, M.G.H. Structure Based Modulation of Electron Dynamics in Meso-(4-Pyridyl)-BODIPYs: A Computational and Synthetic Approach. *J. Phys. Chem. A* **2018**, *122*, 6372–6380. [CrossRef] [PubMed]
24. Zhou, Z.; Maki, T. Ratiometric Fluorescence Acid Probes Based on a Tetrad Structure Including a Single BODIPY Chromophore. *J. Org. Chem.* **2021**, *86*, 17560–17566. [CrossRef]
25. Ndung'u, C.; LaMaster, D.J.; Dhingra, S.; Mitchell, N.H.; Bobadova-Parvanova, P.; Fronczek, F.R.; Elgrishi, N.; Vicente, M.d.G.H. A Comparison of the Photophysical, Electrochemical and Cytotoxic Properties of Meso-(2-, 3- and 4-Pyridyl)-BODIPYs and Their Derivatives. *Sensors* **2022**, *22*, 5121. [CrossRef]
26. Ndung'U, C.; Bobadova-Parvanova, P.; LaMaster, D.J.; Goliber, D.; Fronczek, F.R.; Vicente, M.d.G.H. 8(Meso)-Pyridyl-BODIPYs: Effects of 2,6-Substitution with Electron-Withdrawing Nitro, Chloro, and Methoxycarbonyl Groups. *Molecules* **2023**, *28*, 4581. [CrossRef]
27. Yanai, T.; Tew, D.P.; Handy, N.C. A New Hybrid Exchange–Correlation Functional Using the Coulomb-Attenuating Method (CAM-B3LYP). *Chem. Phys. Lett.* **2004**, *393*, 51–57. [CrossRef]
28. Bauernschmitt, R.; Ahlrichs, R. Treatment of Electronic Excitations within the Adiabatic Approximation of Time Dependent Density Functional Theory. *Chem. Phys. Lett.* **1996**, *256*, 454–464. [CrossRef]
29. Frisch, M.J.; Trucks, G.W.; Schlegel, H.B.; Scuseria, G.E.; Robb, M.A.; Cheeseman, J.R.; Scalmani, G.; Barone, V.; Mennucci, B.; Petersson, G.A.; et al. *Gaussian 09*, Revision D.01; Gaussian, Inc.: Wallingford, CT, USA, 2009.
30. Silva-Junior, M.R.; Schreiber, M.; Sauer, S.P.A.; Thiel, W. Benchmarks for Electronically Excited States: Time-Dependent Density Functional Theory and Density Functional Theory Based Multireference Configuration Interaction. *J. Chem. Phys.* **2008**, *129*, 104103. [CrossRef]

31. Laurent, A.D.; Jacquemin, D. TD-DFT Benchmarks: A Review. *Int. J. Quantum Chem.* **2013**, *113*, 2019–2039. [CrossRef]
32. Nguyen, A.L.; Bobadova-Parvanova, P.; Hopfinger, M.; Fronczek, F.R.; Smith, K.M.; Vicente, M.G.H. Synthesis and Reactivity of 4,4-Dialkoxy-BODIPYs: An Experimental and Computational Study. *Inorg. Chem.* **2015**, *54*, 3228–3236. [CrossRef] [PubMed]
33. Goliber, D.; Hernandez, E.; Lamaster, D.; Vicente, M.; Bobadova, P. Computational Modeling of a Series of 8(meso)-pyridyl-BODIPYs. 2024. Available online: https://scimeetings.acs.org/exhibit/Poster-Board-1616-Computational-modeling/3990974 (accessed on 20 September 2024).
34. Goliber, D.; Hernandez, E.; Bobadova, P. Substituent Effects on the Photophysical Properties of a Series of meso-Pyridyl-BODIPYs: A Computational Analysis of the Experimental Data. 2024. Available online: https://graduatedivision.ucmerced.edu/sites/graduatedivision.ucmerced.edu/files/page/documents/22nd_mercury_program_2024_4.pdf (accessed on 20 September 2024).